J. Fluid Mech. (1972), *vol.* 52, *part* 1, *pp.* 17–31
Printed in Great Britain

Super-Alfvénic supersonic flow over a cone in aligned fields

By LEE A. BERTRAM
Department of Engineering Mechanics, Iowa State University
AND Y. M. LYNN
Division of Mathematics, University of Maryland, Baltimore County

(Received 6 May 1971)

Super-Alfvénic supersonic aligned magnetogasdynamic flow over a cone of finite semi-apex angle, with an attached fast shock wave, is solved numerically. We obtain 'almond curves' in the plane of magnetic induction vector variation, analogous to Busemann's 'apple curves' for supersonic cone flows, to describe the flow field near the cone. Total surface pressure coefficients, current and vorticity distributions are presented. A closed-form solution of the flow is obtained when a switch-on shock occurs.

1. Introduction

The basic problem of magnetogasdynamic flow over a wedge has been studied by Kogan (1959), Cabannes (1963), Chu & Lynn (1963), Mimura (1963) and Pack & Swan (1966). It serves to illustrate various important shock-wave properties but gives plane current and vorticity of infinite extent, as well as uniform current-free flow away from the shock. A physically more realistic and basic problem in hyperbolic aligned magnetogasdynamics is the flow over a semi-infinite non-conducting cone. This is the simplest axisymmetric magnetogasdynamic flow in which the current and vorticity sheets are closed, while its theoretical predictions can readily be subjected to concrete experimental verification.

Sakurai (1962), who numerically investigated the aligned magnetogasdynamic flow over a non-slender cone, obtained mainly non-physical solutions with unstable attached shocks and singular flows. Bausset (1963) has obtained first-order perturbation solutions for aligned magnetogasdynamic flow over thin cones; however, his solutions are valid only for super-Alfvénic flows and he examined shock behaviour only.

This paper presents numerical solutions to the exact equations of motion for aligned super-Alfvénic hyperbolic flow over a semi-infinite cone of finite semi-apex angle, at zero incidence with an attached fast shock wave. The Taylor–Maccoll (1933) solution for supersonic cone flow is contained as a special case. The necessary shock properties and the conical flow equations are given in § 2. It is shown that no conical sub-Alfvénic flow solution exists because of the appearance of an 'embedded characteristic surface' in the flow, while super-Alfvénic

supersonic flow solutions always exist. Numerical solutions for super-Alfvénic supersonic flow over a cone are presented in § 3. In addition to these numerical solutions an exact solution is obtained when switch-on shocks occur.

2. Equation of motion and shock waves

The equations of motion for steady flow of a non-dissipative conducting perfect gas with the magnetic induction vector $\mathbf{B}^+$ aligned with the velocity vector $\mathbf{q}^+$ everywhere are

$$\nabla\cdot(\rho^+\mathbf{q}^+) = 0, \tag{2.1}$$

$$\nabla\times\{(1-1/A^2)\,\mathbf{q}^+\} = 0, \tag{2.2}$$

$$\mathbf{B}^+ = \alpha^+\rho^+\mathbf{q}^+, \tag{2.3}$$

$$\tfrac{1}{2}q^{+2}+\gamma p^+/(\gamma-1)\rho^+ = \text{constant on each streamline}, \tag{2.4}$$

$$p^+/\rho^{+\gamma} = \text{constant on each smooth streamline}, \tag{2.5}$$

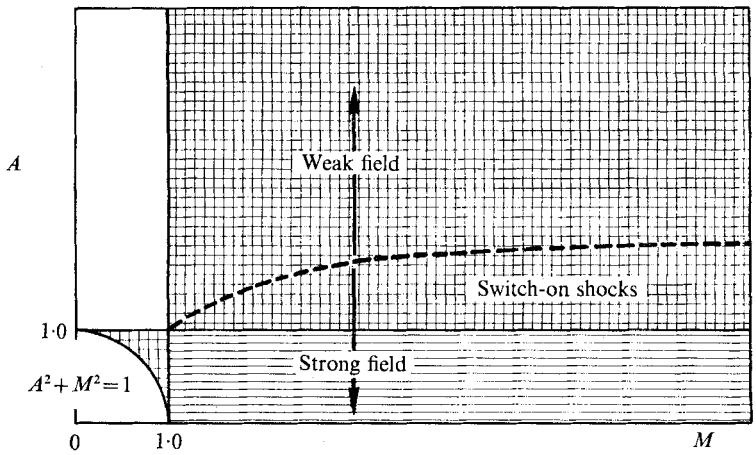

Figure 1. A–M diagram. $\gamma = \frac{5}{3}$; |||, hyperbolic upstream flow ($\lambda^2 > 0$); ≡, evolutionary and thermodynamically admissible shock waves; – – –, $A^2 = (\gamma+1)M^2/[2+(\gamma-1)M^2]$.

where the superscript + denotes all physical variables, α^+ is a constant on each streamline, and ρ^+, p^+ and γ are, respectively, the density, pressure and adiabatic exponent of the gas. The square of the Alfvén number, A^2, is defined by q^{+2}/b^{+2}, where $b^{+2} = B^{+2}/(\mu\rho^+)$ is the square of the Alfvén-wave speed and μ is the constant permeability. Taniuti (1958) and Resler & McCune (1959) have shown that (2.1)–(2.5) are hyperbolic if and only if the quantity

$$\lambda^2 = (M^2-1)\,(A^2-1)/(A^2+M^2-1)$$

is positive. This is illustrated in the A–M diagram in figure 1, where M is the Mach number q^+/a^+, $a^+ = [(\partial p^+/\partial\rho^+)_{s^+}]^{\frac{1}{2}}$ being the gasdynamic sound-wave speed. This behaviour is also easily seen from the characteristic locus, first illustrated by Friedrichs & Kranzer (1954, 1958), as shown in figure 2. Two different systems of parametric expressions for this locus were given by Bazer & Fleishman

(1959) and Weitzner (1961); Lynn (1962) has obtained a single equation to describe this characteristic locus. Standing waves (i.e. the tangents to the characteristic locus (McCune & Resler 1960; Sears 1960) from the terminal of the vector $-\mathbf{q}$) exist only for fast hyperbolic flow, $A > 1$, $M > 1$, and for slow hyperbolic flow, $A < 1, M < 1, A^2+M^2 > 1$. In particular, it is clear from figure 2 that the fast waves are oblique and that the flow speed exceeds both Alfvén- and

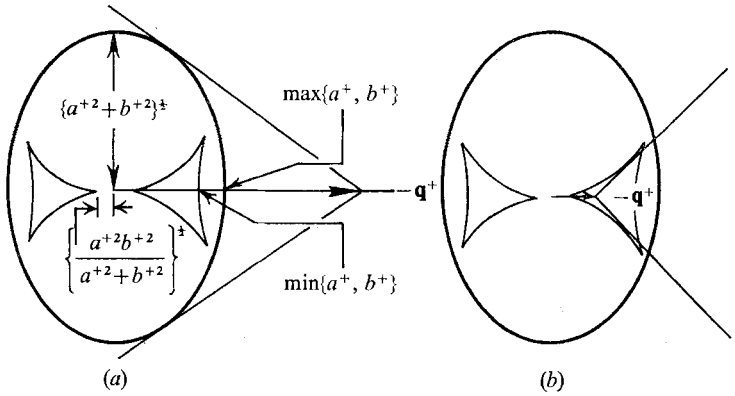

FIGURE 2. Characteristic locus in aligned flow (schematic). (*a*) Fast standing waves in super-Alfvénic supersonic flow. (*b*) Slow standing waves in sub-Alfvénic hyperbolic flow.

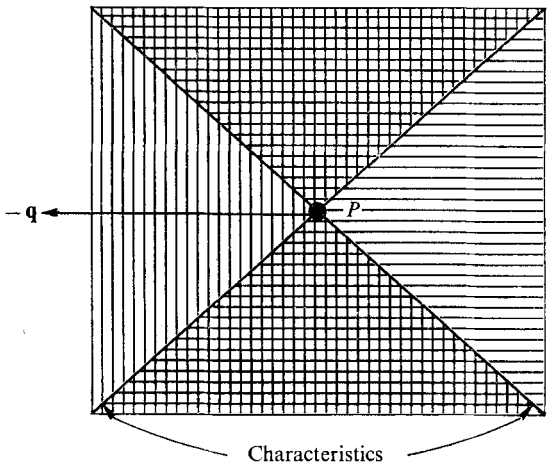

FIGURE 3. Region of influence (horizontal hatching) and domain of dependence (vertical hatching) of a point P in sub-Alfvénic hyperbolic flow.

sound-wave speeds; thus, the upstream flow of fast waves is undisturbed. On the other hand, slow waves are obtuse (upstream-facing) and may have disturbed flow preceding them for the incompressible case as suggested by Stewartson (1960), since both wave speeds exceed the local velocity. In fact, in slow hyperbolic flow, the 'region of influence' and 'domain of dependence' of a point P overlap as shown in figure 3, where the flow variables at any point in the doubly hatched region must both depend on and influence the values at P. The inter-

dependence is qualitatively that of a system described by elliptic equations of motion.

Let $\mathbf{B}_\infty^+$ and $\mathbf{B}^+$ denote the magnetic induction vector ahead of and behind the shock wave respectively. We define $\bar{B} = |\mathbf{B}^+|/|\mathbf{B}_\infty^+| = B^+/B_\infty^+$ and $\xi = \cos\sigma$, where σ is the angle between the vectors $\mathbf{B}_\infty^+$ and $\mathbf{B}^+$. From the system of conservation laws governing state variables across a standing magnetogasdynamic shock wave in steady flows, Lynn (1971) has obtained for aligned fields the equation for the magnetic induction polar (i.e. the magnetogasdynamic shock polar given in terms of magnetic induction polar variables $\bar{B}$ and σ):

$$\begin{aligned} M_\infty^2 \bar{B}(\bar{B}^2-1)(\bar{B}-\xi)^2 + (A_\infty^2-1)\{(\bar{B}-\xi)(\bar{B}\xi-1)[M_\infty^2(2-\gamma)\bar{B}(\bar{B}-\xi) \\ + (2A_\infty^2+\gamma M_\infty^2)(\bar{B}\xi-1)] + \bar{B}(1-\xi^2)[2A_\infty^2(1-M_\infty^2)\bar{B}(\bar{B}-\xi) \\ + (\gamma+1)M_\infty^2(A_\infty^2-1)(\bar{B}^2-2\bar{B}\xi+1)]\} = 0. \end{aligned} \tag{2.6}$$

The graph of (2.6) was first obtained by Kogan (1962) by numerically solving the system of conservation laws. It admits the simple and useful geometrical relation that the line connecting the point (1, 0) and the terminal of the vector $\bar{\mathbf{B}} = \mathbf{B}^+/B_\infty^+$ immediately gives the shock wave inclination as characterized by the angle β measured from the direction of $\mathbf{B}_\infty^+$, as well as that of $\mathbf{q}_\infty^+$. For the super-Alfvénic supersonic upstream flows considered here, the shock polar in the $\bar{B}, \sigma$ plane satisfies both the entropy non-decrease condition (Lüst 1955; Friedrichs & Kranzer 1954, 1958; Ericson & Bazer 1960) and the evolutionary condition (Akhiezer, Lyubarskiĭ & Polovin 1958) if and only if (Lynn 1971)

$$\bar{B}\xi \geqslant 1.$$

This excludes all trans-Alfvénic shocks, which are obtuse-angled and non-evolutionary; only acute-angled and fast shocks are admissible. Again these results may be obtained with considerable effort from Bazer & Ericson (1962). Depending on whether the shock wave with $\beta = \frac{1}{2}\pi$ is a pure gasdynamic normal shock or a switch-on shock, we may classify the fast-shock polars into two distinct types. For aligned fields, the shock wave with $\beta = \frac{1}{2}\pi$, and hence $\bar{B}\xi = 1$, corresponds to the special case with a normal upstream magnetic induction vector, as well as normal upstream velocity vector. Setting $\bar{B} = \xi^{-1}$ in (2.6) gives either

$$\sigma = 0, \tag{2.7a}$$

or

$$\tan^2\sigma = (\gamma+1)(A_\infty^2-1)(1-A_\infty^2/A_s^2), \tag{2.7b}$$

where $A_s = [(\gamma+1)/(\gamma-1+2/M_\infty^2)]^{\frac{1}{2}}$. Since $A_\infty > 1$ for fast shocks, we obtain from (2.7*b*) that the angle σ is real and non-zero only if

$$A_s > A_\infty > 1, \tag{2.8}$$

which corresponds to a switch-on shock. We use condition (2.8) to define 'strong field', as shown in figure 1; the condition also characterizes the upstream states for which switch-on shocks occur. The condition has been derived by Urashima & Morioka (1966), using a different method, and it can also be obtained from the results of Bazer & Ericson (1962). Equation (2.7*b*) can also be obtained immediately by setting $s = 0$ in either equation (C 26) or equation (24) of Lynn (1966),

which hold for standing magnetogasdynamic shock waves in general non-aligned flows (the notations ξ^2, M_i^2/k_i and k_i in the latter reference corresponding respectively to our variables $\tan^2\sigma = \bar{B}^2 - 1$, A_∞^2 and M_∞^2/A_∞^2). Thus the complete set of solutions for a switch-on shock is immediately available by taking a simple limit of the solution given in Lynn (1966). In particular, we set $s = 0$ in equation (C 24) of Lynn's paper and get $\bar{\rho} = A_\infty^2$, which yields

$$A^2 = 1 \tag{2.9}$$

since $A_\infty^2 = \bar{\rho}A^2$ follows from (2.3). Equation (2.9) shows that the flow behind a switch-on shock is always Alfvénic. From (2.4) and (2.7 *b*)

$$\frac{1}{M^2} - 1 = \frac{\gamma+1}{2\bar{B}^2 A_s^2}[(\gamma+2)A_\infty^4 - (\gamma+1)(A_s^2+1)A_\infty^2 + \gamma A_s^2],$$

which indicates that flow behind a switch-on shock can be either subsonic, if

$$A_s > A_\infty > A_d, \tag{2.10a}$$

or supersonic, if

$$A_d > A_\infty > 1, \tag{2.10b}$$

where $$A_d^2 = A_s^2\left\{1 + \gamma M_\infty^2 + \left[\frac{2\gamma}{\gamma+1}M_\infty^2(M_\infty^2-1)+1\right]^{\frac{1}{2}}\right\}\{(\gamma+2)M_\infty^2\}^{-1}.$$

The magnitudes of the jumps in all thermodynamic variables decrease monotonically with increasing field strength for the switch-on shock.

In contrast to the inequality (2.8), consider the case of $A_\infty > A_s > 1$, which is used to define 'weak fields', as shown in figure 1. The only other solution possible is $\sigma = 0$ in (2.7 *a*); this corresponds to a pure-gasdynamic normal shock wave (Lynn 1966; Urashima & Morioka 1966). Since $A^2 = A_\infty^2/\bar{\rho} = A_\infty^2/A_s^2 > 1$ in our case, we conclude that the flow behind a gasdynamic normal shock is always subsonic and super-Alfvénic. The strong-field polar is simply a portion of the typical weak-field polar truncated at the normal shock – see figures 8 and 9 for typical polars of each type.

Now, writing (2.1)–(2.5) for a homentropic conical flow in spherical co-ordinates (figure 4) gives

$$d\sigma/d\theta = \kappa\cos(\sigma-\theta)\sin\sigma/E\sin\theta, \tag{2.11}$$

$$dq/d\theta = q(A^2-1)\sin(\sigma-\theta)\sin\sigma/(A^2M^2E\sin\theta), \tag{2.12}$$

where $$\kappa = (A^2+M^2-1)/A^2M^2 = (1+\lambda^2)^{-1}, \quad E = \sin^2(\sigma-\theta) - \kappa,$$

$$A^2 = A_\infty^2/\rho, \quad M^2 = q^2\rho/p,$$

$$\rho = \{H[1+\tfrac{1}{2}(\gamma-1)(M_\infty^2-q^2)]\}^{1/(\gamma-1)},$$

$$p = \rho^\gamma/H. \tag{2.13}$$

In terms of the dimensionless variables

$$\mathbf{B} = \mathbf{B}^+/(\gamma\mu p_\infty^+)^{\frac{1}{2}} = (M_\infty/A_\infty)(\mathbf{B}^+/B_\infty^+) = \rho\mathbf{q}/A_\infty,$$

$$p = p^+/p_\infty, \quad \mathbf{q} = \mathbf{q}^+/a_\infty^+, \quad \rho = \rho^+/\rho_\infty,$$

and $H = \bar{p}/\bar{\rho}^\gamma = \exp[(s^+ - s_\infty^+)/c_v]$, where s^+ is the specific entropy of the gas and c_v is the specific heat at constant volume. The current density

$$\mathbf{j} = \nabla\times\mathbf{B} = \mathbf{j}^+L^+/(\gamma\rho_\infty^+/\mu)^{\frac{1}{2}}$$

and vorticity

$$\boldsymbol{\zeta} = \mathbf{j}/A_\infty = \boldsymbol{\zeta}^+L^+/a_\infty^+$$

may be non-dimensionalized by any length L^+ since the non-dissipative conical flow has no characteristic length. The semi-infinite cone boundary-value problem now consists of finding solutions to (2.11)–(2.12) which are subject to the boundary condition

$$\sigma(\theta_c) = \theta_c, \tag{2.14}$$

where the subscript c refers to the cone surface, and of finding a shock angle β such that relation (2.6) is satisfied at $\theta = \beta$.

The equations of motion, (2.11) and (2.12), will be singular whenever E vanishes; this occurs for

$$\sin^2(\sigma - \theta) = \kappa = \sin^2\omega^{\pm} \tag{2.15}$$

if and only if the inclination $(\sigma - \theta)$ of the vector $\mathbf{q}$ to a ray θ is characteristic, i.e. equal to $\omega^{\pm}$, where the $\pm$ superscripts denote acute and obtuse roots of (2.15) respectively. Since it can be shown from the shock relationships that a stable compressive shock lies between the upstream and downstream characteristic inclinations, $\omega_\infty - \sigma < \beta - \sigma < \omega$, evidently the fast hyperbolic shock 'cuts off' the downstream characteristics, and E is negative just behind the shock. Since E is also negative on the cone surface by (2.14) and has no zeros between shock and cone (Bertram 1969) the equations are nowhere singular in a fast hyperbolic flow.

For slow hyperbolic flow with obtuse shock angles, E is positive just behind the shock, but (2.14) again requires $E(\theta_c) < 0$. Thus E vanishes somewhere between the shock and cone, and the slow hyperbolic flow always has an 'embedded characteristic' lying on some conical surface $\theta = \theta^*$. It can be shown that there is no continuous solution across this surface unless the downstream flow is uniform and parallel to the axis; this flow would consist of uniform flow, terminated by a shock, followed by a non-uniform conical flow and, downstream of θ^*, a uniform flow again, with no cone downstream of the shock. Such a flow is non-physical, so no sub-Alfvénic hyperbolic conical flow can exist.

In summary, despite the fact that the sub-Alfvénic (slow) shock waves satisfy the evolutionary condition, which is necessary but not sufficient to guarantee physical existence (see, for example, Lynn 1966), the cone boundary-value problem with attached shocks in this case has no solution if the downstream flow is hyperbolic. Thus Sakurai's (1962) numerical results shown in his figure 7 (corresponding to point 1 of his figure 1) apparently result from numerical error since they are slow-hyperbolic flows, while those in his figure 8 (corresponding to point 2 in his figure 1) all have non-evolutionary shocks, as do all of those in figures 10 and 11 (corresponding to points 6 and 7) with obtuse shock angles. These latter are trans-Alfvénic shocks.

3. Numerical solution for flow over a non-slender cone

To obtain numerical solutions to the cone boundary-value problem, we solve (2.11)–(2.14) by converting to an initial-value problem. This is done by specifying A_∞, M_∞, γ and the shock angle β, then solving the shock relations for initial values, and integrating until (2.14) is satisfied (see appendix for further detail).

Solutions were obtained in the groups given in table 1, with $\gamma = \frac{5}{3}$ in all cases; these are shown in figure 5.

The resulting solutions differ from gasdynamic conical flow because there is vorticity and current present, and because switch-on shocks appear in the strong-field case. Current density and vorticity are related by

$$\mathbf{j} = \nabla \times \mathbf{B} = \nabla \times ((A_\infty / A^2)\,\mathbf{q}) = A_\infty \nabla \times \mathbf{q} = A_\infty \boldsymbol{\zeta} = \mathbf{j}(r, \theta), \tag{3.1}$$

Fixed $\theta_c = 5°$	Fixed upstream state with different values of β, hence different values of θ_c
Series 1: $M_\infty = 2$, $1{\cdot}0 \leqslant A_\infty \leqslant 20$	Series 4: $A_\infty = M_\infty = 2$, $\omega_\infty^+ < \beta \leqslant \frac{1}{2}\pi$
Series 2: $A_\infty = 2$, $1{\cdot}1 \leqslant M_\infty \leqslant 20$	Series 5: $A_\infty = 1{\cdot}1$, $M_\infty = 2$, $\omega_\infty^+ < \beta \leqslant \frac{1}{2}\pi$
Series 3: $1{\cdot}05 \leqslant A_\infty = M_\infty \leqslant 20$	

TABLE 1

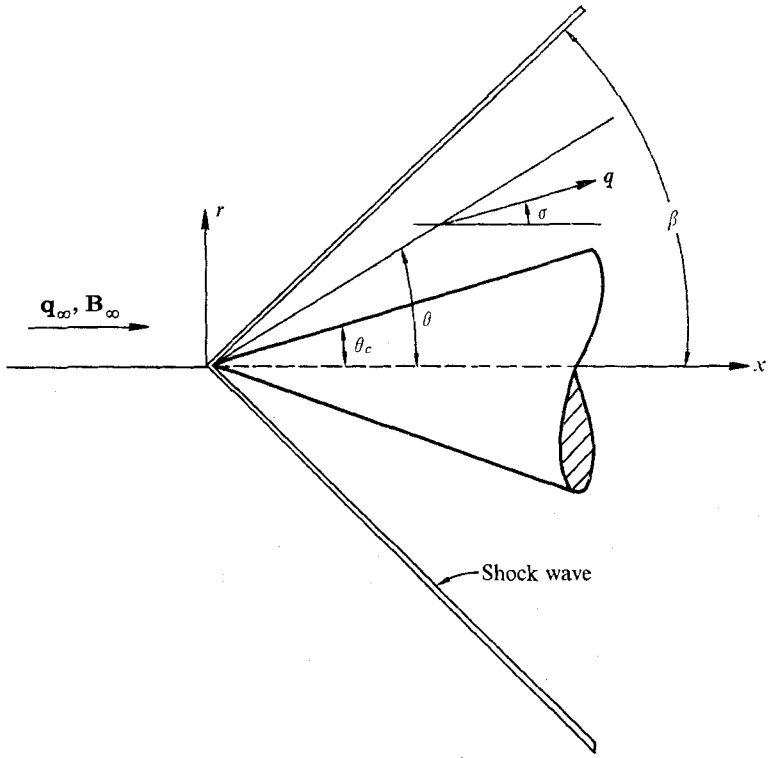

FIGURE 4. Super-Alfvénic supersonic cone flow.

where r is the cylindrical co-ordinate in figure 4 and equations (2.2) and (2.3) have been used. Now,

$$\mathbf{j}(r, \theta) = [(1/r)\rho q \sin^2(\sigma - \theta) \sin\sigma / (2A_\infty E)]\,\mathbf{e}_\phi = (1/r) j(\theta)\,\mathbf{e}_\phi, \tag{3.2}$$

$\mathbf{e}_\phi$ being the azimuthal unit vector. Altogether, the following currents are present.

(i) Shock current sheet: $\mathbf{J}_s = \mathbf{n}_s \times (\mathbf{B}_t - \mathbf{B}_{t_\infty})$; current/length; positive azimuthal sense.

(ii) Flow current density: $\mathbf{j}(r,\theta)$ given by (3.2); current/area; positive azimuthal sense.

(iii) Cone-surface current sheet: $\mathbf{J}_c = \mathbf{n}_c \times \mathbf{B}_c$; current/length; negative azimuthal sense.

$\mathbf{n}_s$ and $\mathbf{n}_c$ refer to the unit vector normal to the shock and cone respectively. Pack & Swan (1966) have identified the cone-surface current sheet as a degenerate shock of non-aligned flow.

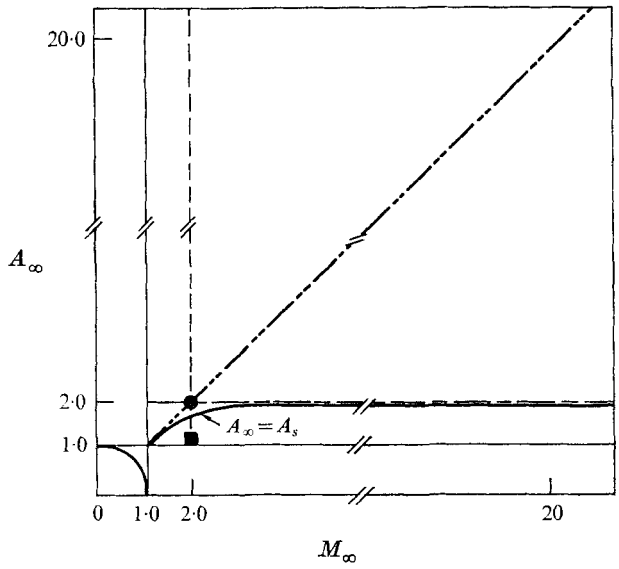

FIGURE 5. Input for numerical solutions (not to scale). ———, series 1; —·—, series 2; —··—, series 3; ●, series 4; ■, series 5.

The level lines of $\mathbf{j}(r,\theta)$ are shown for $(A_\infty, M_\infty, \gamma) = (2{\cdot}0, 2{\cdot}0, \frac{5}{3})$ in figure 6 for a typical weak shock, $\beta = 42°$, in the upper half and for a typical strong shock, $\beta = 89{\cdot}5°$, in the lower half of the figure. The total current J flowing between two such level lines $j_2 \leqslant |\mathbf{j}(r,\theta)| \leqslant j_1$ is

$$J = \int_{\theta_c}^{\beta} \int_{R_1(\theta,j_1)}^{R_2(\theta,j_2)} |j(R,\theta)|\, R\, dR\, d\theta = \int_{\theta_c}^{\beta} \frac{j(\theta)}{\sin\theta} (R_2 - R_1)\, d\theta$$

$$= \left(\frac{1}{j_2} - \frac{1}{j_1}\right) \int_{\theta_c}^{\beta} \left(\frac{j(\theta)}{\sin\theta}\right)^2 d\theta = \left(\frac{1}{j_2} - \frac{1}{j_1}\right) g(\beta, \theta_c, A_\infty, M_\infty, \gamma),$$

where $R = r/\sin\theta$ = the spherical radial co-ordinate. The total current between each pair of level lines in either half of figure 6 is twice as large as that between the next pair of level lines toward the apex.

The current sheets in the shock and on these cones are, respectively, 0·01918 and $-1{\cdot}077$ for the weak shock, and 0·02617 and $-0{\cdot}9629$ for the strong shock. Thus, everywhere except in the shock itself, the weak-shock solution has the more intense currents and distributes them more uniformly throughout the flow.

In the case of a switch-on shock (2.11) and (2.12) may be solved explicitly. Since $A = 1$ just behind the shock,

$$dq/d\theta = q(A^2-1)\sin(\sigma-\theta)\sin\sigma/A^2M^2E\sin\theta, \tag{3.3}$$

$$d\sigma/d\theta = -\sin\sigma/\sin\theta\cos(\sigma-\theta). \tag{3.4}$$

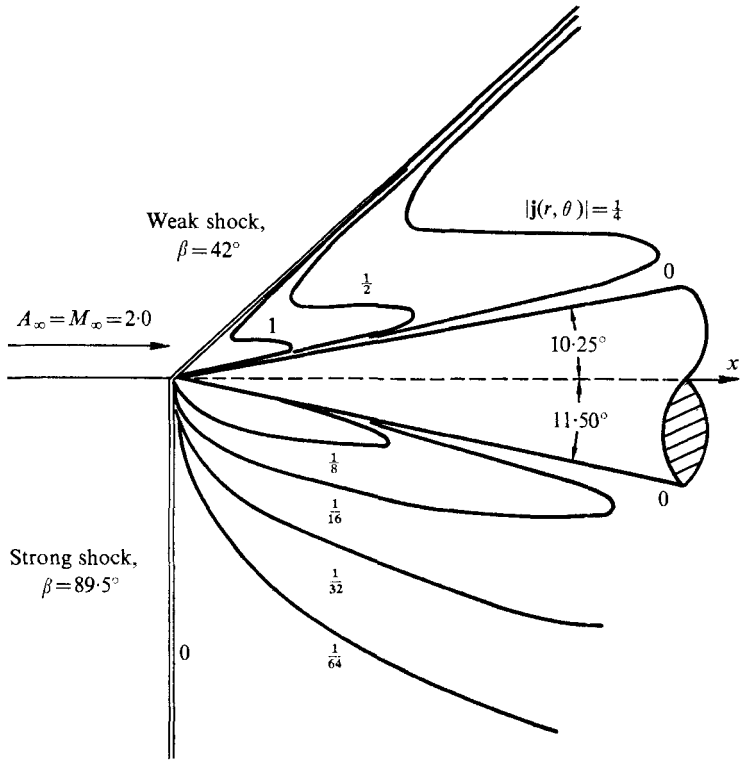

FIGURE 6. Current density in super-Alfvénic supersonic cone flow.

Continued differentiation of (2.12) shows that $d^nq/d\theta^n = 0$ for $A = 1$, so the fact that $A = 1$ at one point on a streamline implies that q is a constant on the streamline, unless a shock cuts the streamline. However, a shock with Alfvénic upstream conditions must be a switch-off shock (Friedrichs & Kranzer 1958) and the converse is also true (Lynn 1971). Since switch-off shock angles are always obtuse (Bazer & Ericson 1962), which would imply intersecting shock waves and non-conical flow, we conclude that the entire region behind the shock has $A = 1$.

The solution to (3.3) and (3.4) is then

$$q = \text{constant} = [1/A_\infty^4 + (\gamma+1)(1-1/A_\infty^2)(1/A_\infty^2 - 1/A_s^2)]^{\frac{1}{2}}, \tag{3.5}$$

$$f(\sigma,\theta) = \text{constant} = \cot\theta/\sin\sigma + \ln[(1+\cos\sigma)/\sin\sigma]$$

$$= f(\theta_c,\theta_c) = f(\sigma(\tfrac{1}{2}\pi),\tfrac{1}{2}\pi), \tag{3.6}$$

where (3.5) follows from the shock solutions and (3.6) from integration of (3.4). Each level line of $f(\sigma,\theta)$ in the σ, θ plane is a solution curve; these are shown in figure 7. The particular level line for a given problem is chosen by evaluating f

either on a given cone surface or by calculating $\sigma(\frac{1}{2}\pi)$ from (2.7*b*) when the upstream state is given.

The analogue to Busemann's 'apple curve' (Busemann 1929) may be constructed in the magnetic induction plane, with points on the shock polar for a fixed A_∞, M_∞ and γ mapped onto points of the 'almond curve' as shown in figures 8 and 9,

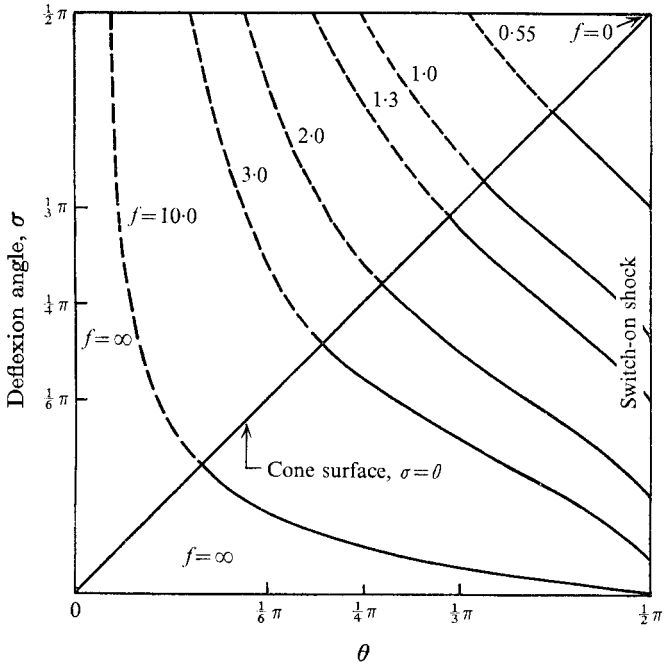

FIGURE 7. Alfvénic cone flows.

where 'cone-flow isentrope' refers to a solution of (2.11) and (2.12). Weak- and strong-field forms of the almond curve, like those of the shock polars, are respectively open and closed curves, owing to the evolutionary criterion.

Figure 8 displays the shock polar and almond curve for a typical weak-field case, series 4. On the polar, each $\sigma(\beta)$ corresponds to both a strong- and a weak-shock solution, separated by the point $\sigma = \sigma_{\max}$. When the shock angle here is larger than 73°, the intense shock will produce sonic transition; i.e. $M(\beta) < 1$ for $\beta > 73°$, so (2.11) and (2.12) are elliptic for the strong-shock branch of this polar. Similarly, on the almond curve each θ_c has two solutions for $\theta_c < \theta_{c,\max}$. The strong-shock solution here has the entire disturbed flow elliptic because of the shock-produced sonic transition. The weak-shock solution is either all fast hyperbolic or has an embedded elliptic region from the cone surface out into the flow, because the combined shock and isentropic compression produces $M_c < 1$ for $\beta > 69°$. Although such embedded elliptic regions have been observed experimentally in gasdynamic cone flows (Solomon 1954) their stability in magnetogasdynamic flow is unknown.

The strong-field polar and the almond curve for series 5 are shown in figure 9. For this polar $A_\infty < A_d$, so all flows are supersonic and super-Alfvénic behind

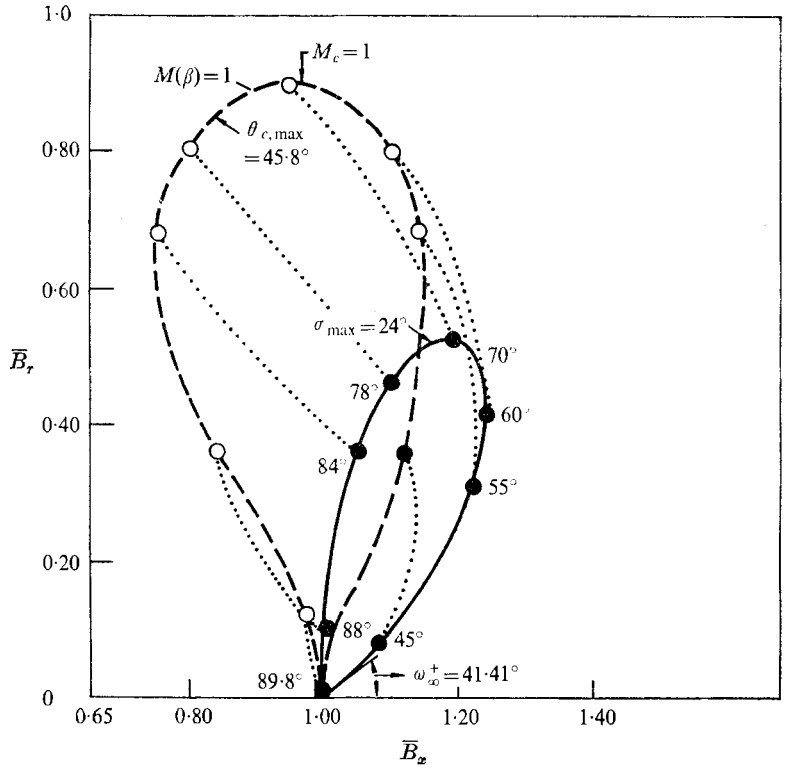

FIGURE 8. Weak-field almond curve. $(A_\infty, M_\infty, \gamma) = (2{\cdot}0, 2{\cdot}0, \frac{5}{3})$. ——, shock polar; ·····, cone-flow isentrope; – – –, almond curve.

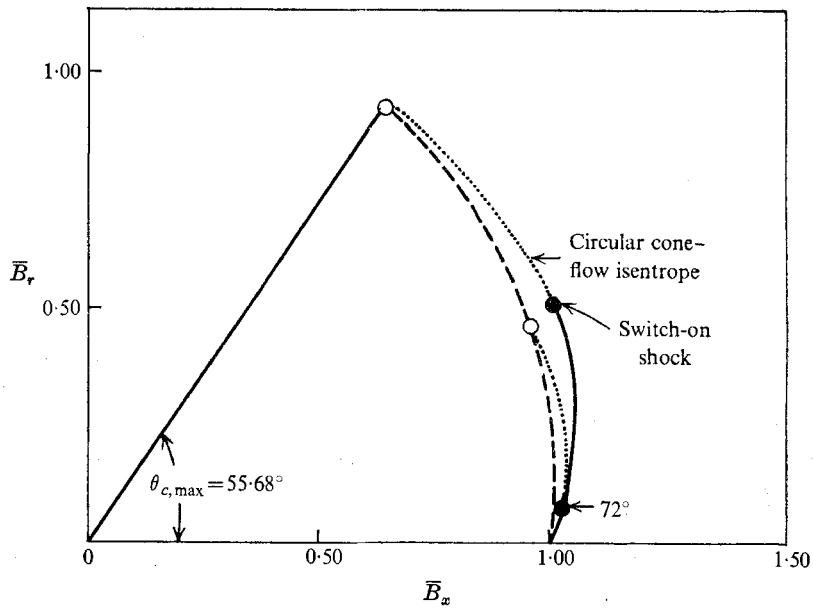

FIGURE 9. Strong-field almond curve. $(A_\infty, M_\infty, \gamma) = (1{\cdot}1, 2{\cdot}0, \frac{5}{3})$. ——, shock polar; ·····, circular cone-flow isentrope; – – –, almond curve.

the shocks, except for the switch-on, which has $A(\beta) = 1, M(\beta) > 1$. The resulting almond curve has $M_c > 1$ at all points and ends at the switch-on cone-flow solution, which has the maximum cone angle at which a shock may remain attached for this A_∞, M_∞, and γ. The switch-on cone-flow isentrope is circular because q = constant implies that $\rho, \bar{B}$ = constant, according to (2.3) and (2.4). Note that the shock–isentropic compression of any cone flow is incapable of producing Alfvénic transition because a shock can at most reduce A to unity and no isentropic compression can then follow because of (3.3), which also requires that a smooth streamline has $A = 1$ everywhere or nowhere on it. This is in contrast to the sonic transitions occurring in the weak-field cone flows.

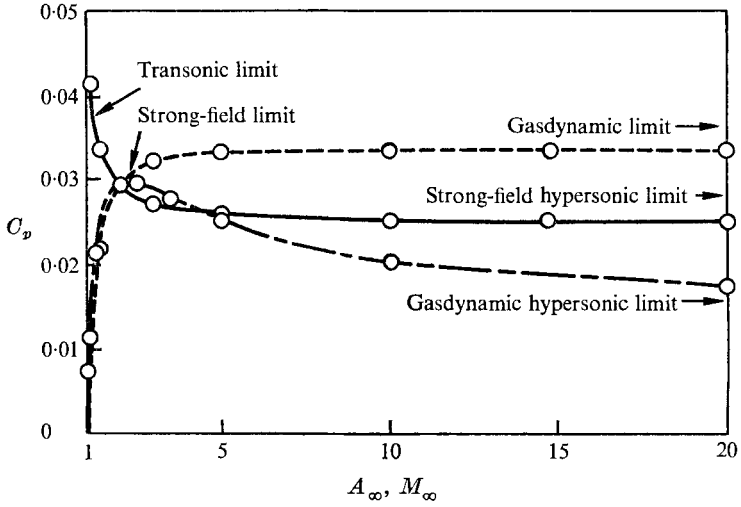

FIGURE 10. Pressure coefficient for a 5° cone. ——, $A_\infty = 2$; —·—, $A_\infty = M_\infty$; – – –, $M_\infty = 2$; ○, computed point.

The remaining numerical calculations, series 1–3, were made with θ_c fixed at 5°; the influence of A_∞ and M_∞ on the total pressure coefficient

$$C_p = \left[\left(p^+ + \frac{B^{+2}}{2\mu}\right)_c - \left(p_\infty^+ + \frac{B_\infty^{+2}}{2\mu}\right)\right] [\tfrac{1}{2}\rho_\infty^+ q_\infty^{+2}]^{-1} \tag{3.7}$$

is displayed in figure 10. In all calculations only the weak-shock solution was calculated. The cone angle was controlled to only four significant figures because the numerical error analysis in the appendix indicates that this is the precision of the shock-to-cone integration.

The curve in figure 10 for fixed field strength $A_\infty = 2$ is of the same form as that from gasdynamics, which includes the vertical tangent where it joins the strong-shock solution branch near transonic conditions. However, C_p reaches a non-zero asymptotic value as M_∞ becomes large unlike the gasdynamic case. Note that the curve in figure 5 on which these upstream states lie approaches the strong-field boundary $A_\infty = A_s$ at large M_∞. At these M_∞ values, C_p is independent of M_∞; the flow, like the shock, is dominated by the field as A_∞ approaches A_s.

The curve in figure 10 for a fixed $M_\infty = 2$ plainly shows that increasing field strength decreases C_p, just as the switch-on shock pressure ratio decreases at stronger field strength. The decrease in C_p is smooth from $A_\infty = \infty$ down to $A_{\infty,\text{switch-on}}$, at which point the nose shock is a switch-on shock; at $A_{\infty,\text{switch-on}}$, (2.13), (3.5) and (3.7) give

$$C_{p,\text{switch-on}} = 2(1 - 1/A^2_{\infty,\text{switch-on}}). \tag{3.8}$$

For slender cones $A_{\infty,\text{switch-on}}$ is very close to unity and, according to (3.6), $A_{\infty,\text{switch-on}} \simeq 1 + 10^{-97}$ for $\theta_c = 5°$, which will lead to $C_{p,\text{switch-on}} \simeq 4 \times 10^{-97}$.

The final curve in figure 10, $A_\infty = M_\infty$, includes values given in figure 5 from the gasdynamic hypersonic limit down to the field-dominated double transition at $A_\infty = M_\infty = 1$. 'Field-dominated' refers to the fact that the curve tends towards zero as transition is approached like the constant M_∞ curve, rather than turning upward as the fixed field-strength curve does.

One of us (L. A. B.) gratefully acknowledges the financial support of NDEA Title IV fellowship and of Ford Foundation during this work, and partial support by the Engineering Research Institute.

Appendix. Numerical stability and error

The initial-value problem [equations (2.11)–(2.14)] is integrated from shock to cone in preference to forward integration in order that the maximum precision of the variables occur in the region where the sensitivity to error is greatest – at the shock wave, when E and σ are both minimum. The program for this integration begins by inversion of the shock relations with a Newton–Raphson method. This solution is specified to have eight significant figures. A fourth-order Runge–Kutta integrator, with variable step size chosen so that the two mid-interval estimates of the derivatives match to 10^{-5}, is then used to integrate until the boundary condition is satisfied.

Karim (1966) has analysed the stability of this integrator when applied to a system of equations with a fixed step size. Stability is guaranteed if $\Delta\theta e_i$ falls into a particular region of the complex-e_i plane, where e_i are the eigenvalues of the Jacobian matrix

$$\tilde{J} = \begin{vmatrix} \partial\sigma'/\partial\sigma & \partial\sigma'/\partial q \\ \partial q'/\partial\sigma & \partial q'/\partial q \end{vmatrix} \tag{A 1}$$

evaluated in (θ_{n-1}, θ_n), where primes indicate $d/d\theta$.

The partial derivatives indicated are

$$\partial\sigma'/\partial\sigma = [-\tan(\sigma-\theta) + \cot\sigma - \sin^2(\sigma-\theta)/E]\,\sigma',$$

$$\partial q'/\partial\sigma = [\cot(\sigma-\theta) + \cot\sigma - \sin 2(\sigma-\theta)/E]\,q',$$

$$\partial\sigma'/\partial q = [\kappa_1 \sin^2(\sigma-\theta)/\kappa E]\,\sigma',$$

$$\frac{\partial q'}{\partial q} = \left[\frac{A^2M^2\kappa}{A^2-1} - 2N + \kappa_1 q/E\right] \times \frac{q'}{q},$$

where

$$\kappa_1 = \partial\kappa/\partial q = -[2N(A^2-1) + M^2(M^2-1)]/(A^2M^2q),$$

$$N = 1 + \tfrac{1}{2}(\gamma-1)\,M^2.$$

When the e_i values are real, the stability interval is

$$-2{\cdot}785\ldots < \Delta\theta e_i < 0 \quad (i = 1, 2). \tag{A 2}$$

It can be shown that the partial derivatives in (A 1) have the same behaviour for any super-Alfvénic flow, so the stability analysis was carried out only for the typical case $(A_\infty, M_\infty, \gamma, \beta) = (5, 2, \frac{5}{3}, 31{\cdot}966568°)$. It is found that the eigenvalues are real, negative and of order one except near the shock, where both complex values, with real and imaginary parts order ten or less, and large values of different signs, appear. The resulting small $O(10^{-3})$ values of $\Delta\theta e_i$ imply an essentially neutrally stable integration over most of the interval, while the mixed signs near the shock wave leave the stability ambiguous; both of these statements are true regardless of the direction of the integration.

For a stable integration, the error $\boldsymbol{\epsilon}_n$ at the nth step is bounded by

$$\boldsymbol{\epsilon}_n < -\left[\sum_{\nu=1}^{4} \frac{(\Delta\theta\tilde{J})^\nu}{\nu!}\right]^{-1} \mathbf{R}, \tag{A 3}$$

where $\mathbf{R}$ is the difference between round-off error and truncation error, due to the method of integration. With the nearly neutral integration it may be inferred that the error is of this order. Conservatively taking $\mathbf{R}$ to be $O(10^{-5})$, that is, the order of the mid-interval derivative difference, and noting that $\Delta\theta J_{ij} = O(1)$ at worst, (A 3) gives an error of $O(10^{-5})$. This estimate is confirmed by comparing runs with all inputs fixed except the minimum step size; when $|\Delta\theta_{\min}| \leqslant \frac{1}{32}°$ results agree to four significant figures.

REFERENCES

Akhiezer, A. J., Lyubarskiĭ, G. I. & Polovin, R. V. 1958 *Zh. éksp. teor. Fiz.* **35**, 731. (Trans. in *Soviet Phys. JETP*, **8**, 507.)

Bausset, M. 1963 *C. r. hebd. Séanc. Acad. Sci., Paris*, **257**, 372.

Bazer, J. & Ericson, W. B. 1962 *Proc. Symp. on Electromagnetics & Fluid Dyn. of Gaseous Plasma*, Microwave Res. Inst. Symp. Series, vol. xi, p. 387. Brooklyn: Polytech. Press.

Bazer, J. & Fleishman, O. 1959 *Phys. Fluids*, **2**, 366.

Bertram, L. A. 1969 Ph.D. thesis, Illinois Institute of Technology.

Busemann, A. 1929 *Z. angew. Math. Mech.* **9**, 496.

Cabannes, H. 1963 *C. r. hebd. Séanc. Acad. Sci., Paris*, **257**, 375.

Chu, C. K. & Lynn, Y. M. 1963 *A.I.A.A. J.* **1**, 1062.

Ericson, W. B. & Bazer, J. 1960 *Phys. Fluids*, **3**, 631.

Friedrichs, K. O. 1954 *Los Alamos Rep.* LAMS-2105.

Friedrichs, K. O. & Kranzer, H. 1958 *New York Univ. Courant Inst. Math. Sci. Rep.* NYO-6486-VIII.

Kalikhman, L. E. 1967 *Elements of Magnetogasdynamics*, p. 142. W. B. Saunders.

Karim, A. I. A. 1966 *Communs. Ass. comput. Mach.* **9**, 113.

Kogan, M. N. 1959 *Prikh. Mat. Mech. Akad. Nauk SSSR*, **23**, 70. (Trans. in *Appl. Math. Mech.* **23**, 92.)

Kogan, M. N. 1962 *Problems of Magnetohydrodynamics and Plasma Dynamics*, p. 54. Academy of Science Latvian SSR. (Trans.: see Kalikhman 1967.)

Lüst, R. 1955 *Z. Naturforschung*, **10**(*a*), 125.

Lynn, Y. M. 1962 *Phys. Fluids*, **5**, 626.

LYNN, Y. M. 1966 *Phys. Fluids*, **9**, 314.

LYNN, Y. M. 1971 *J. Plasma Phys.* **6**, 283.

MCCUNE, J. E. & RESLER, E. L. 1960 *J. Aerospace Sci.* **27**, 493.

MIMURA, Y. 1963 *A.I.A.A. J.* **1**, 272.

PACK, D. C. & SWAN, G. W. 1966 *J. Fluid Mech.* **25**, 165.

RESLER, E. L. & MCCUNE, J. E. 1959 In *The Magnetogasdynamics of Conducting Fluids* (ed. D Bershader), p. 120. Stanford University Press.

SAKURAI, T. 1962 *Proc. 3rd Int. Symp. on Rockets and Astronautics* (ed. S. Saito *et al.*), p. 189. Tokyo: Yokendo Bunkyo-ku.

SEARS, W. R. 1960 *Rev. Mod. Phys.* **32**, 701.

SOLOMON, G. E. 1954 *N.A.C.A.* 3213.

STEWARTSON, K. 1960 *Rev. Mod. Phys.* **32**, 855.

TANIUTI, T. 1958 *Prog. Theor. Phys., Kyoto*, **19**, 749.

TAYLOR, G. I. & MACCOLL, J. W. 1933 *Proc. Roy. Soc.* A **139**, 278.

URASHIMA, S. & MORIOKA, S. 1966 *J. Phys. Soc. Japan*, **21**, 1431.

WEITZNER, H. 1961 *Phys. Fluids*, **4**, 1238.